Waste Management 91 (2019) 1–8

Contents lists available at ScienceDirect

Waste Management

journal homepage: www.elsevier.com/locate/wasman

Lignocellulosic nanofibrils produced using wheat straw and their pulping solid residue: From agricultural waste to cellulose nanomaterials

Huiyang Bian [a], Ying Gao [a], Jing Luo [b], Liang Jiao [a], Weibing Wu [a], Guigan Fang [c], Hongqi Dai [a,*]

[a] Jiangsu Provincial Key Lab of Pulp and Paper Science and Technology, Nanjing Forestry University, Nanjing 210037, China
[b] Jiangsu Co-Innovation Center of Efficient Processing and Utilization of Forest Resources, Nanjing Forestry University, Nanjing 210037, China
[c] China Institute of Chemical Industry of Forestry Products, Chinese Academy of Forestry, Nanjing 210042, China

ARTICLE INFO

Article history:
Received 19 March 2019
Revised 24 April 2019
Accepted 25 April 2019
Available online 28 April 2019

Keywords:
Agricultural residue waste
Wheat straw
Waste wheat straw
Delignification
Mechanical fibrillation
Lignocellulosic nanofibrils

ABSTRACT

Each year millions of tons of agricultural wastes are produced, however, not well utilized in China. Considering the economic development and environmental protection, the valorization of these wastes is increasingly necessary and important. Here we used *p*-toluenesulfonic acid hydrolysis followed by mild disk grinding for on-farm valorization of wheat straw (WS) and their pulping solid residue (waste wheat straw, WWS) to produce lignocellulosic nanofibrils (LCNF). Alkaline peroxide post-treatment was further conducted to obtain purified lignocellulosic nanofibrils (P-LCNF) with lower lignin content and thinner diameters. The raw materials and resulting LCNF and P-LCNF were investigated in each process for their chemical component, crystal structure, morphology, and thermal properties. Interestingly, although WS fiber had higher lignin content than WWS fiber, the WS fiber with lower ash content resulted in LCNF and P-LCNF with smaller height and lower thermal stability, but higher crystallinity and higher specific surface area. Higher ash content in WWS fiber protected cellulose and lignin from depolymerization and degradation, respectively, which endowed LCNF and P-LCNF with entangled network structure. Overall, this study indicated that the low-temperature fractionation process on WS and WWS fibers could yield cellulose nanomaterials with potential value-added application and achieve the efficient utilization of agricultural wastes.

1. Introduction

Lignocellulosic biomass, in the form of wood, grasses, industrial waste, and agricultural residues, represent the most abundant and renewable resource worldwide (de Hoyos-Martinez et al., 2018; Hietala et al., 2018; Rajinipriya et al., 2018; Zhu et al., 2016). Due to higher cost of wood-based cellulosic resources, recent scientific and technological advances in the area of new materials have stressed the importance of using agricultural waste as a resource of raw material, especially in developing countries with large agricultural production (Chen et al., 2014; Cypriano et al., 2018; Jebali et al., 2018; Shi et al., 2018). It is estimated that about 80 million tons of wheat straw (WS) are produced every year in China, making it the most abundant agricultural residues in the country (Huang et al., 2016). However, only a limited percentage of WS is used in the pulping industry due to the severe environmental issues and the difficulties in economic alkali recovery. These residues are usually buried in soil or burnt in the field because this is the quickest and cheapest approach to prepare fields for the coming cropping season (Liu et al., 2017). This approach may cause air pollution and potential fire risk. Moreover, waste wheat straw (WWS), the solid residue remaining as a byproduct from the WS pulping industry, are more difficult to utilize efficiently due to its more complex composition (Huang et al., 2016). Therefore, economic and effective utilization of these agricultural waste residues is the key to achieve environmental friendliness. Although WS and WWS have lower cellulose content than that of wood raw materials, these annually renewable residues have shorter growth cycles with a moderate risk level, giving them a great potential in high value-added products (Ardanuy et al., 2012; Tarrés et al., 2017).

So far, various methods have been applied to produce lignocellulosic nanofibrils (LCNF) from WS. These strategies facilitated the effective solubilization of some chemical components such as cellulose, hemicellulose and lignin, beneficial for subsequent mechanical treatment with low energy input (Alemdar and Sain,

* Corresponding author. Tel.: 86-25-85428932.
E-mail address: hgdhq@njfu.edu.cn (H. Dai).

https://doi.org/10.1016/j.wasman.2019.04.052
0956-053X/

2008; Barbash et al., 2017; Liu et al., 2017). The main issues of the studies that have been reported include: (1) the neutralization of chemicals and the difficulties in economic chemical recovery; (2) high demand of reaction temperature and pressure during the whole treatments; (3) the low thermal stability of the resultant lignin-free cellulose nanofibrils (CNF). It also has been reported that nanofibrillation became very difficult and fiber suspension sometimes clogged in the reaction chamber when using undelignified fibers (Spence et al., 2010a; Rojo et al., 2015). Therefore, one critical issue common to WWS and WS fibers is the lignin content, as high as 20%. Recently, *p*-toluenesulfonic acid (*p*-TsOH), a commercial catalyst, was found to have hydrotropic properties and capability of rapidly solubilizing partial wood lignin in aqueous solutions at low temperatures (Bian et al., 2017). The approach can be used to produce lignocellulosic nanofibrils (LCNF) with hydrophobic properties. Furthermore, LCNF carrying residual lignin, hemicelluloses, and extractives may present an attractive option for higher yield, low production cost, and much lower environmental impact, which showed promising properties for bio-based composite and packaging applications (Farooq et al., 2019; Wang et al., 2018).

Previously, we developed a new approach (including prewashing, *p*-toluenesulfonic acid hydrolysis, disk grinding, and endoglucanase post-treatment) for improving the cellulose nanofibrillation of high ash content WWS (Bian et al., 2018b). The objective of this work is to demonstrate that agricultural residues from WWS and WS fibers can be utilized to produce LCNF directly by *p*-TsOH fractionation and mild mechanical fibrillation, and the alkaline peroxide post-treatment can further decrease lignin content and fibril diameter to meet the market demands for LCNF (Fig. 1). The morphological, physical, and thermal properties of the resulting agricultural waste cellulose nanomaterials were studied and compared in order to assess their potential application.

2. Experimental

2.1. Materials

The wheat straw (WS) and waste wheat straw (WWS) were obtained from a straw pulp mill (LiaoCheng, Shandong, China). *p*-Toluenesulfonic acid (*p*-TsOH) was analytical reagent and purchased from LiFeng Chemical Reagent Co. Ltd., (Shanghai, China). Graphite (99.95% metals basis, 8000 mesh) was supplied by Aladdin Industrial Corporation (Shanghai, China).

2.2. Fractionation of WS and WWS using p-TsOH

Concentrated aqueous *p*-TsOH solution (80 wt%) was prepared by heating the required amounts of acid and de-ionized (DI) water in a three-necked flask at 80 °C (Chen et al., 2017). WS or WWS of 10 g in oven dry (OD) weight were manually added into the acid solution with continuous stirring, resulting in acid solution to sample mass ratio of 10:1 (g/g). The pulp suspensions were constantly agitated at 300 rpm for 20 min. The reaction was then quenched by adding 100 mL of DI-water. The hydrolysate was quickly filtered by a filter paper under vacuum. The filtered solids were washed with DI water and collected for further processing.

2.3. Mechanical fibrillation

Two hydrolyzed fiber samples of approximately 1 wt% concentration were mechanically fibrillated at 1500 rpm to produce LCNF using a stone disk grinder (SuperMassCollodier, Model: MKCA6-2J, Disk Model: MKG-C, Masuko Sangyo Co., Ltd, Japan). The disk gap was first set to zero without pulp, and then with adjusted down to −100 μm. Each sample was fed by gravity through a hopper during fibrillation and passed through the disk chamber for five times.

2.4. Alkaline peroxide post-treatment

The purification procedure performed in this work was based on the method reported by a previous work (Su et al., 2012), in which alkaline peroxide was used. Bleaching was performed at 60 °C by adding the obtained LCNF suspension into 2% H_2O_2 solution followed by mechanical stirring for 12 h. The suspension was adjusted to pH 11.5 with 4 M NaOH in the initial stage of reaction. No further pH adjustments were made during the course of the reaction. The resultant purified LCNF (P-LCNF) was dialyzed using DI water until the pH of the dialysis water no longer changed. Homogeneous fibril suspension at concentration of 1 wt% was poured into a cylindrical plastic tube and frozen in liquid nitrogen (−196 °C) for 15 min. Sample was obtained by freeze-drying under −80 °C for 3 days, then stored at ambient atmosphere for characterization.

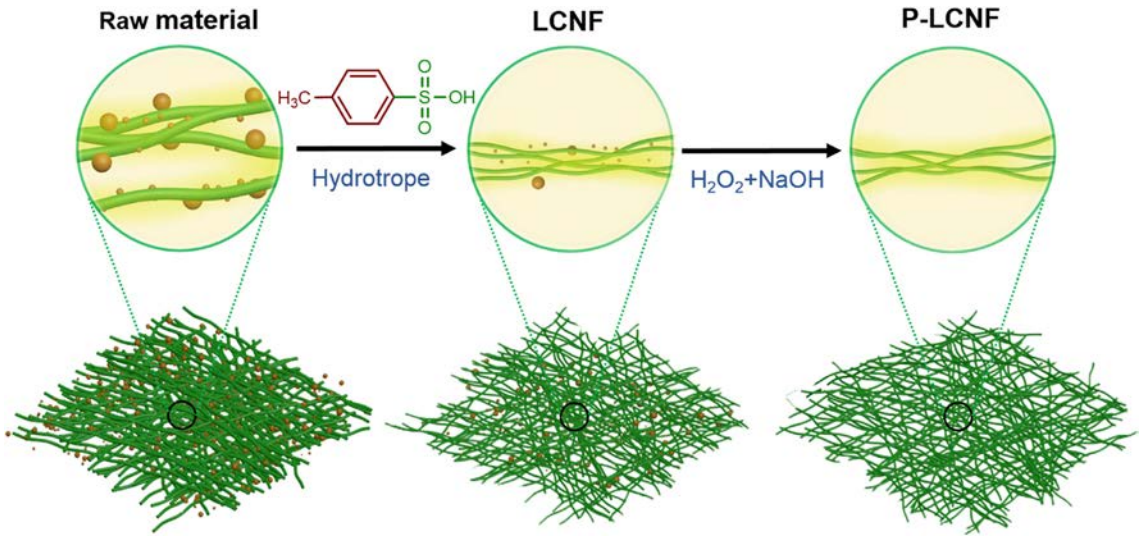

Fig. 1. A schematic flow diagram of experiments for preparing lignocellulosic nanofibrils using agricultural residue wastes.

2.5. Chemical composition

The chemical compositions of raw materials, LCNF and P-LCNF were hydrolyzed using sulfuric acid in two steps for carbohydrate, klason lignin and ash analyses, as described previously (Sluiter et al., 2008a; Sluiter et al., 2008b).

2.6. Morphology observation

The morphologies of the raw materials, LCNF, and P-LCNF were observed using scanning electron microscopy (SEM, Quanta 200, FEI, USA). Samples were dried on a polished aluminum mount and sputter-coated with gold to provide adequate conductivity.

The morphologies of LCNF and P-LCNF were also observed by atomic force microscopy (AFM; Dimension Edge, Bruker, Germany). Specimens were prepared by air drying drops of aqueous slurry of 0.01 wt% onto clean mica substrates. AFM topographical images were scanned in tapping mode at 300 kHz with a radius of curvature of 8 nm. Height distribution was measured with the AFM software (Gwyddion, Department of Nanometrology, Czech Metrology Institute, Crezh Republic, 64-bit).

2.7. Specific surface area

The specific surface area of LCNF and P-LCNF samples were determined using Congo Red (CR) adsorption method, as described previously (Inglesby and Zeronian, 2002; Bian et al., 2018a). Approximately 0.05 g of samples were adjusted to the pH of 6 and dyed with varying amount of CR at solids content of approximately 0.7%. At the beginning of the experiment, the charged surface sites on the original fiber and LCNF were neutralized using a small amount of NaCl (only 0.004 wt%). Samples were incubated at 60 °C for 24 h and then centrifuged at 10000 rpm for 10 min. UV–vis adsorption (Model 8453, Agilent Technologies, Inc., USA) of supernatant samples at 500 nm were measured to determine the CR concentrations using Langmuir's adsorption theory, according to Eq. (1):

$$\frac{[E]}{[A]} = \frac{1}{K_{ad}A_{max}} + \frac{[E]}{A_{max}} \quad (1)$$

where $[E]$ (mg/mL) is the solution concentration of Congo Red at adsorption equilibrium, $[A]$ is the adsorbed amount of Congo red on the cellulose surface in mg/g (that reached a maximum value equivalent to A_{max}, the maximum adsorbed amount), and K_{ad} is the equilibrium constant. The specific surface area was determined according to Eq. (2):

$$SSA = \frac{A_{max} \times N \times SA}{MW \times 10^{21}} \quad (2)$$

where N is Avogadro's constant, SA and MW are the surface area of a single dye molecule (1.73 nm^2) and molecular weight (696 g/mole) of Congo Red, respectively.

2.8. Thermogravimetric analysis (TGA)

Thermogravimetric analyses (TGA) of raw materials, corresponding LCNF and P-LCNF samples were conducted on thermogravimetric analyzer (NETZSCH, TG 209F1, Germany). Samples of roughly 10 mg were heated from 50 °C to 500 °C at a heating rate of 10 °C/min under high purity nitrogen stream of 20 mL/min.

2.9. X-ray diffraction (XRD)

The XRD patterns were measured on a Rigaku-D/MAX instrument (Rigaku Corp., Tokyo, Japan) with Cu-Kα radiation generated at a voltage of 40 kV and a current of 30 mA with a 2θ range of 10–40° in steps of 0.02°. The crystallinity index (CrI) was calculated according to Eq. (3) based on the Segal method (without baseline substrate) (Segal et al., 1959):

$$\mathrm{CrI} = \frac{I_{002} - I_{am}}{I_{002}} \times 100\% \quad (3)$$

2.10. Fourier transform infrared spectroscopy (FTIR)

The FTIR spectra were obtained by a Fourier transform infrared spectrometer (Nicolet 380, USA). Samples were ground into powders and blended with KBr powder, then pressed into a disk at 30 MPa. The spectrum for each sample was recorded in the region of 4000–400 cm^{-1}. All samples were vacuum dried before analyses.

3. Results and discussion

3.1. Chemical composition

Fig. 2 compares the chemical compositions of WS and WWS at different processing stages. Compared to WS, WWS contained higher percentage of ash and lower percentage of cellulose, hemicellulose and lignin. After the *p*-TsOH hydrolysis and mechanical fibrillation, cellulose content increased in WWS-LCNF and WS-LCNF, however, the ash and lignin content decreased. This was because water removed partial free ash and *p*-TsOH could easily donate a proton in an aqueous solution to isolate lignin by breaking glycosidic, ether and ester bonds in carbohydrates, lignin, and lignin-carbohydrate complexes (Bian et al., 2019; Chen et al., 2018). Moreover, the residual lignin content in WWS-LCNF was higher than that of WS-LCNF, this results was attributed to the presence of high ash content in WWS, which might neutralize

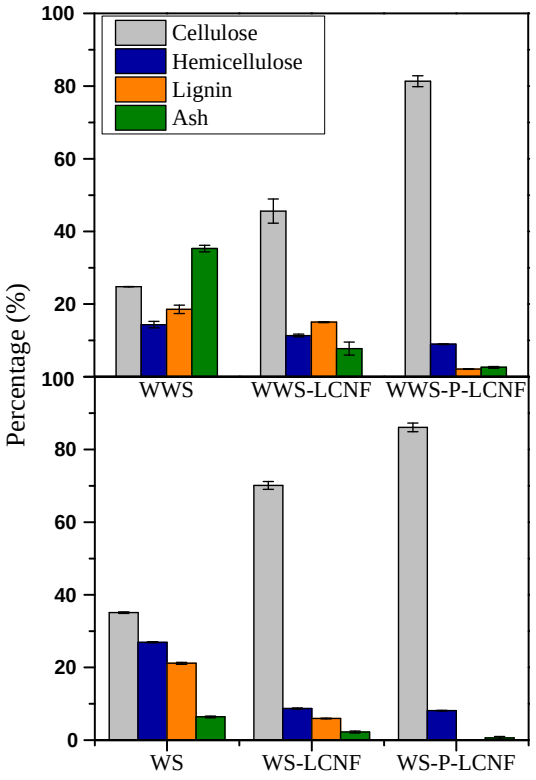

Fig. 2. Chemical composition of WS and WWS fibers, and their corresponding LCNF and P-LCNF.

partial acidic catalysts, resulting in invalid consuming of a substantial amount of acid and low delignification efficiency. Lignin content could be further decreased in both LCNF samples during the alkaline peroxide post-treatment. Overall, the combined treatments removed most of the lignin and ash, enriched the cellulose content with final value of 81.3% and 86.1%, respectively in WWS-P-LCNF and WS-P-LCNF.

FTIR was carried out to investigate the changes in the chemical structure during the whole process. The FTIR spectra of WWS, WS, and corresponding LCNF and P-LCNF samples are shown in Fig. 3. Similar to the results of other works, two main wavenumber regions ranging from 3500 to 2900 and 1750 to 600 cm^{-1} were in all curves. A broad and prominent peak at 3330 cm^{-1} corresponded to the O-H stretching band, while a distinct peak at 2910 cm^{-1} was attributed to C-H stretching vibrations in cellulose and hemicellulose (Kaushik and Singh, 2011). The absorption peaks at 1161 and 896 cm^{-1} in each sample were interpreted as typical cellulose structure. The peak at 1736 cm^{-1} in the spectra of WWS, WS, and two LCNF samples was ascribed to the acetic and uronic ester groups in hemicelluloses and the ester linkages of the carboxylic group of ferulic and *p*-coumaric acid in lignin or hemicelluloses (Chandra et al., 2016), which were virtually absent from the spectra of two P-LCNF samples. This result suggested that the nearly complete cleavage of both hemicellulose and lignin. The peaks at 1250 and 1509 cm^{-1} in WWS and WS fibers corresponded to the aromatic skeletal vibrations of lignin, and were not visible in P-LCNF samples, indicating the reduction in lignin content (Tripathi et al., 2017).

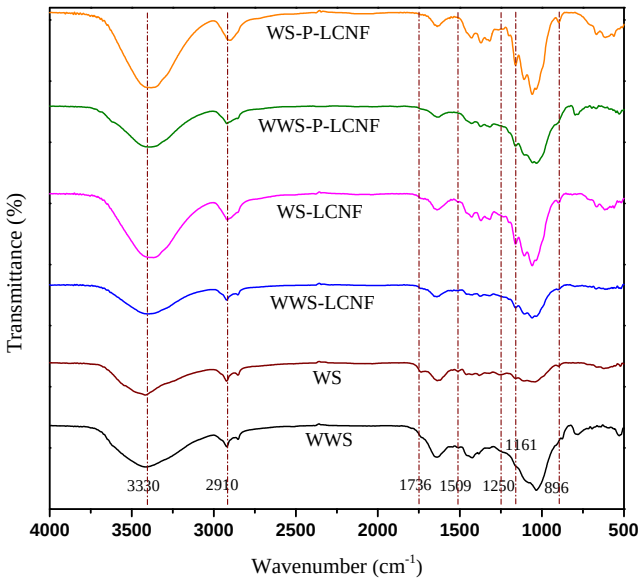

Fig. 3. FTIR spectra of WWS and WS fibers, and their corresponding LCNF and P-LCNF.

3.2. Morphological analysis

The morphologies of the original fibers and corresponding LCNF and P-LCNF were investigated using SEM. Similar to other plant fibers, the raw WWS and WS fibers were regularly arranged and clustered together in bundles from the SEM images (Fig. 4b and 4g). The fiber bundles were loosened after acid hydrolysis due to the degradation of a portion of hemicellulose and lignin molecules from the inner parts of the fiber, thus facilitating the defibrillation during the grinding process (Fig. 4c–d and 4h–i). It was apparent that thinner fibrils could be obtained after the post-purification because the residual lignin adhered to the individual fibril was removed by alkaline peroxide, which was evident from the chemical analyses (Fig. 4e and 4j). Moreover, LCNF and P-LCNF obtained from WS were thinner with large amounts of porous structure in the SEM micrographs, compared with those isolated from WWS. This was perhaps due to the presence of higher lignin and ash content in WWS, impeding mechanical fibrillation and chemical purification as demonstrated previously (Bian et al., 2018b).

To eliminate the influence of self-aggregation on the diameters of fibrils during freeze-drying process, the morphologies of LCNF and P-LCNF were also observed using AFM images (Fig. 5). Some small, globular-shaped lignin particles were clearly visible in both of LCNF samples, in agreement with a previous study (Herrera et al., 2018). Similar type of spherical structures was also seen in SEM images (Fig. 4c and 4g). Subsequent purification resulted in less entangled P-LCNF with thinner diameters as observed from Fig. 5b and 5e and AFM measured height distributions (Fig. 5c and 5f). The number averaged height for the WWS-P-LCNF and WS-P-LCNF were 47.2 nm and 11.8 nm, respectively, lower than those LCNF samples without post-purification with height of 85.3 nm and 27.3 nm (Table 1). Moreover, the distribution became narrower or more uniform, suggesting delignification facilitated nanofibrillation, consistent with the results found in the literature using medium density fiberboard fibers to produce LCNF (Bian et al., 2017).

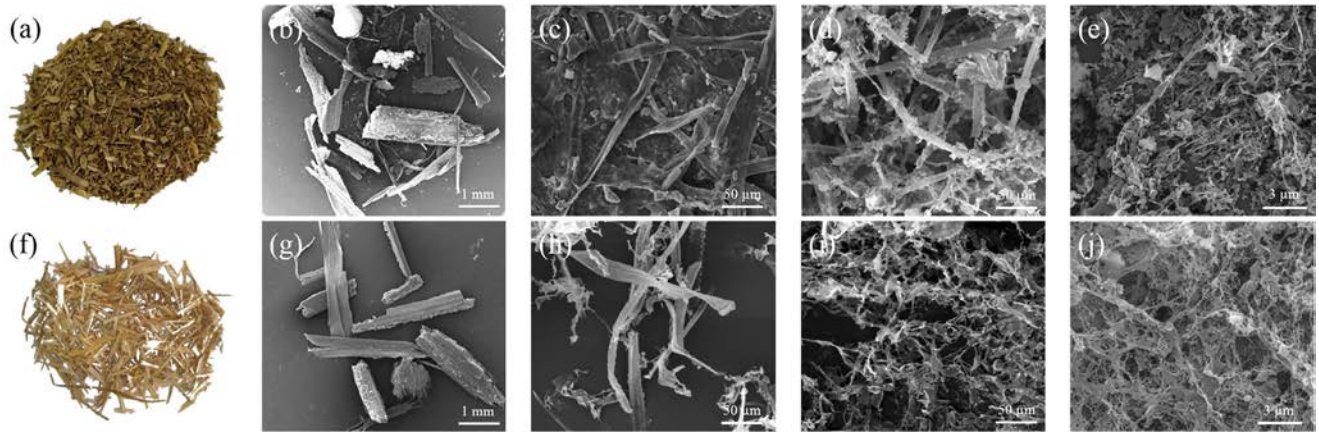

Fig. 4. Photographs of input materials of (a) WWS and (f) WS for lignocellulosic nanofibrils production. Scanning electron microscopy (SEM) images of the WWS and WS after various treatments containing acid hydrolysis, mechanical fibrillation and post-purification. (b) WWS; (c) acid hydrolyzed WWS fiber; (d) WWS-LCNF; (e) WWS-P-LCNF; (g) WS; (h) acid hydrolyzed WS fiber; (i) WS-LCNF; (j) WS-P-LCNF.

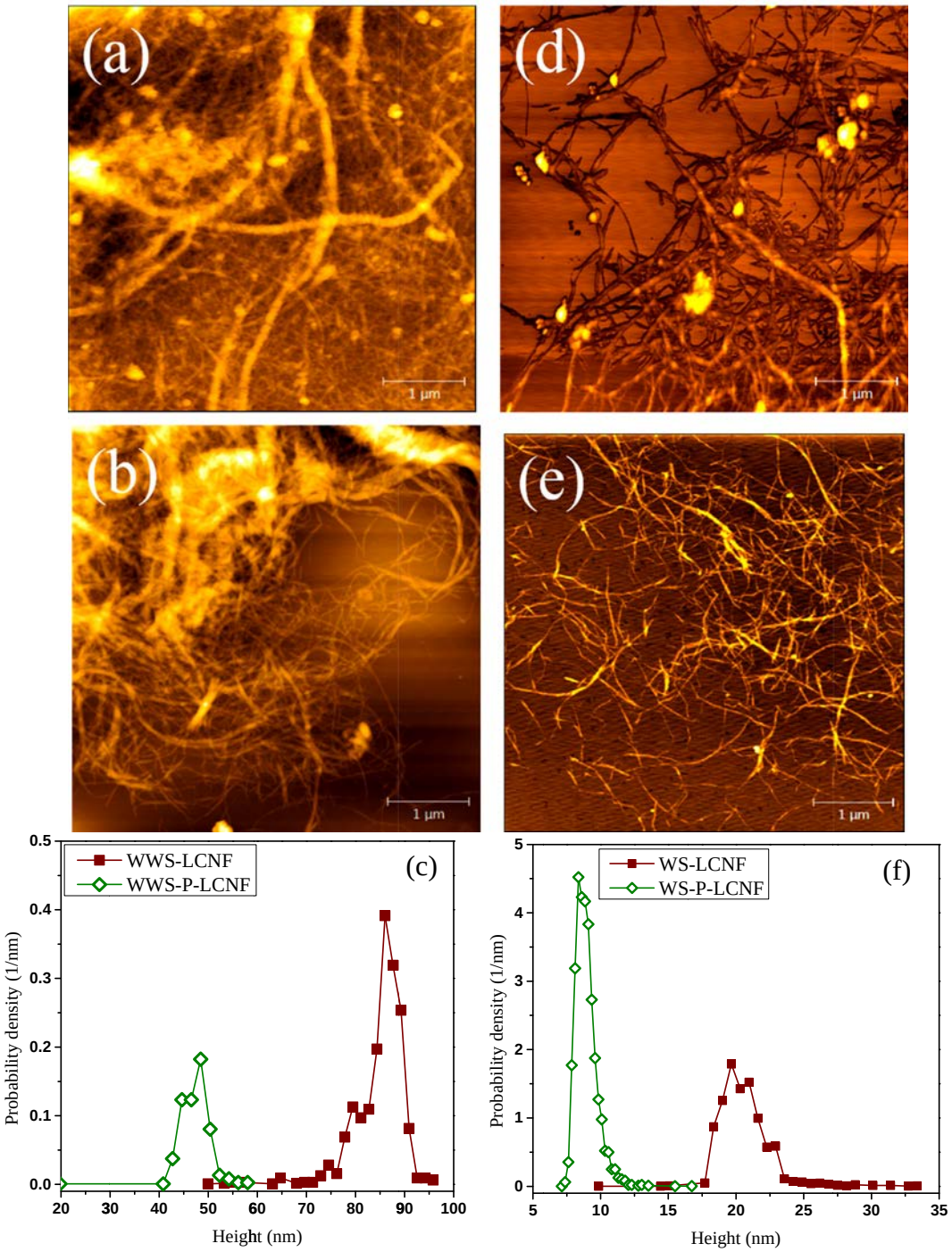

Fig. 5. AFM images of different LCNF and P-LCNF samples from WWS and WS fibers. (a) WWS-LCNF; (b) WWS-P-LCNF; (d) WS-LCNF; (e) WS-P-LCNF. Scale bar = 1 μm. (c) Comparison of the AFM measured WWS-LCNF and WWS-P-LCNF fibril height distribution. (f) Comparison of the AFM measured WS-LCNF and WS-P-LCNF fibril height distribution.

Table 1
List of morphological, physical, and thermal properties of lignocellulosic nanofibrils (LCNF), and purified lignocellulosic nanofibrils (P-LCNF) prepared from WWS and WS fibers.

Sample label	Average height (nm)	CrI (%)	SSA (m^2/g)	T_{max} (°C)	Residue at 600 °C (%)
WWS	–	50.1	6.8 ± 1.1	342	68.2
WWS-LCNF	85.3	58.3	24.0 ± 1.9	341	53.0
WWS-P-LCNF	47.2	69.5	40.5 ± 3.8	347	36.4
WS	–	53.1	37.4 ± 4.3	325	30.2
WS-LCNF	27.3	63.5	325.0 ± 6.1	334	31.8
WS-P-LCNF	11.8	73.5	467.1 ± 9.9	332	26.8

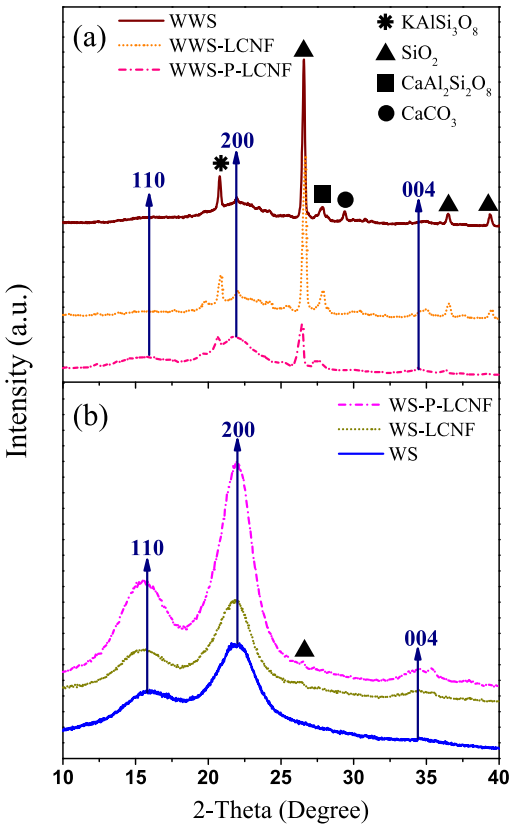

Fig. 6. XRD patterns of WWS and WS fibers, and their corresponding LCNF and P-LCNF.

3.3. Properties of LCNF and P-LCNF

XRD patterns were shown at each treatment stage of the WWS and WS fibers to investigate the changes in crystallinity. The comparison of XRD profiles for WWS and WS fibers are shown in Fig. 6a and 6b, respectively. All diffractograms had three characteristic peaks at about 16.4°, 22.6° and 34.5°, corresponding to the (1 1 0), (2 0 0), and (0 0 4) reflection planes of typical cellulose I structure (Agarwal et al., 2017). For the patterns of WWS fiber, there were four major diffraction peaks, which were assigned to silica, $KAlSi_2O_3$, $CaAl_2Si_2O_8$, and $CaCO_3$, representing the main component from WWS ashes. It should be noted that 7.76% and 2.62% of the ash could not be completely removed in WWS-LCNF and WWS-P-LCNF after sequential treatments, these residual ashes were mainly structural silica (shown in Fig. 6a). Compared to WWS fiber with complex chemical composition, ash in WS fiber was mainly in the form of silica with very low content. To quantitatively compare the changes in crystalline structure for WS and WWS fibers, the values of the CrI estimated from XRD are summarized in Table 1. Despite it is generally accepted that mechanical fibrillation may break up cellulose crystals to reduce cellulose crystallinity, *p*-TsOH hydrolysis dissolved substantial amounts of amorphous hemicellulose and lignin, which resulted in the increase in measured CrI of LCNF. Compared with two LCNF samples, the CrI values for the WWS-P-LCNF and WS-P-LCNF were higher because of the more efficient dissolution of amorphous lignin after the alkaline peroxide treatment. Moreover, WS-P-LCNF had the highest CrI value of 73.5% among all samples, perhaps due to lowest content of lignin and ash. These results provided support for our suggestion that WS fibers are more suitable materials for downstream LCNF production.

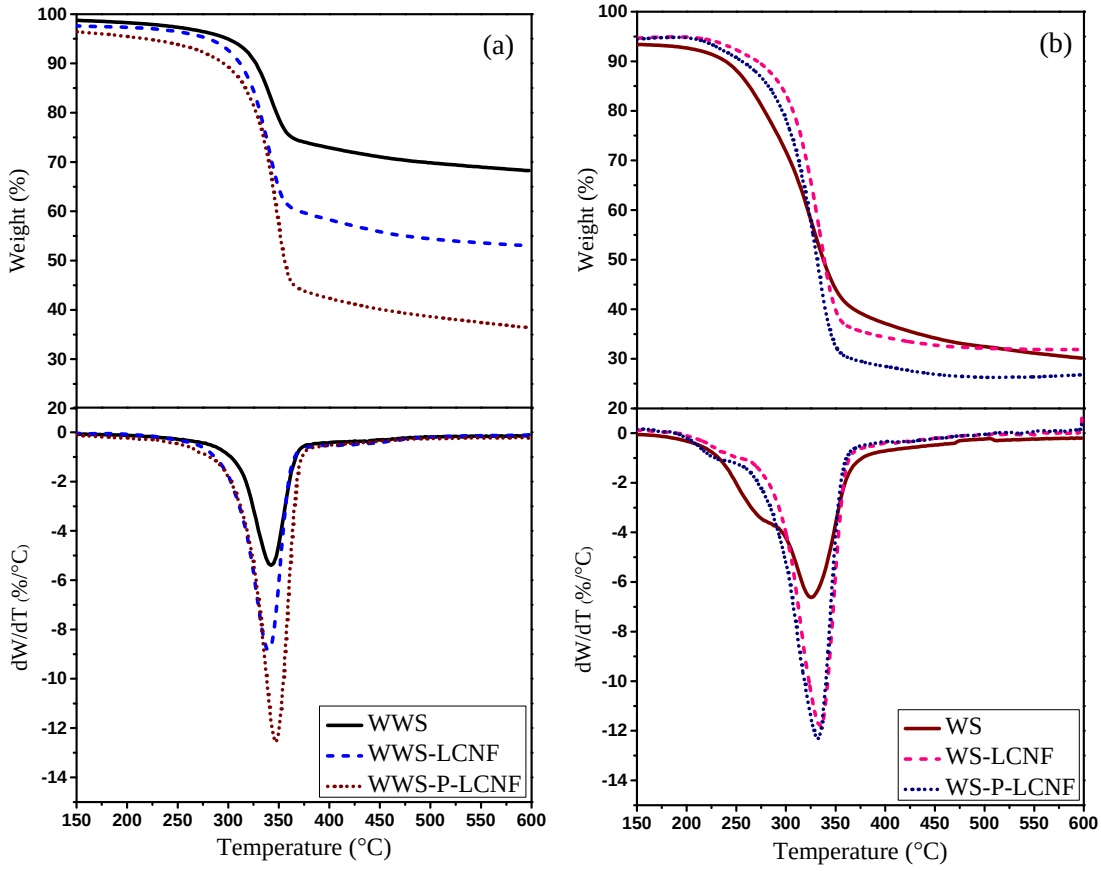

Fig. 7. Comparison of thermal stability of WWS and WS fibers and corresponding LCNF and P-LCNF samples. (a) TGA weight loss; (b) TGA temperature derivative weight loss.

Specific surface area (SSA) of substrate is calculated by Congo red (CR) adsorption using Langmuir-type isotherms since it is an indirect indicator of the degree of fibrillation. When cellulose fibers were defibrillated into nano-scaled fibrils, the SSA was increased due to the change in external surface and internal pore structure of the fibrils (Spence et al., 2010b). As expected, the WWS-LCNF only had SSA of 24.0 m^2/g, lower than its corresponding P-LCNF sample with SSA of 40.5 m^2/g. LCNF and P-LCNF samples isolated from WS fiber exhibited up to 13-fold and 11-fold increase in SSA over that from WWS fiber, respectively (Table 1). This result was attributed to smaller diameter of fibril, as observed in AFM images. Thus, it seemed that amorphous component in raw material and degree of fibrillation might affect the adsorption of CR molecules on cellulose surface.

The thermal properties of cellulose nanomaterials are crucial to their intended use in biocomposites, insulation or packaging materials (Oliveira et al., 2016). TGA was performed to investigate the thermal stability and degradation characteristics of the WWS and WS fibers at various stages of treatment. The thermogravimetric (TG) and derivative thermogravimetric (DTG) curves of the raw materials, LCNF, and P-LCNF are shown in Fig. 7a and 7b. The maximal weight loss temperature (T_{max}) derived from the DTG data, and the residual mass at 600 °C are also listed in Table 1. Due to difference in the chemical structure among cellulose, hemicelluloses and lignin, they presented different thermal stabilities. Compared to other samples, WWS fiber was highest in ash and lignin content, resulting in the largest residual mass of 68.2% at 600 °C. The residual mass of LCNF and P-LCNF samples decreased significantly at 600 °C because of the removal of large amounts of lignin and ash. Our previous study reported that lignin was thermally more stable than cellulose and hemicelluloses, thereby, samples with higher lignin content presented better thermal stability (Bian et al., 2017). However, in the case of WWS-P-LCNF and WS-P-LCNF samples, they had higher T_{max} of 347 °C and 332 °C, respectively, perhaps that the higher crystalline structure caused higher degradation temperatures. Therefore, the higher temperature of thermal decomposition and lower residual mass of the LCNF samples are related to the removal of hemicellulose, lignin and ash from the fibers, as well as the higher crystallinity of cellulose.

4. Conclusion

This study demonstrated the potential for sustainable valorization of wheat straw and their pulping solid residue for producing lignocellulosic nanofibrils through multistep processes that combined *p*-TsOH hydrolysis, disk grinding, and purification post-treatment. The raw materials and obtained LCNF and P-LCNF samples were compared to better understand the effect of each treatment on the chemical composition, morphology, crystalline structure, and thermal behavior. Based on the comparative analysis of the component and morphology, it was shown that the lower lignin and ash content in fibers, the more uniform and thinner fibrils of the resulting LCNF and P-LCNF. The pathway we presented here has a substantial impact on high value utilization of the agricultural residue wastes, as well as for environmental protection.

Acknowledgments

This work was supported by the National Natural Science Foundation of China (Project No. 31470599) and the Doctorate Fellowship Foundation of Nanjing Forestry University. We also would like to acknowledge Jing Yang and Buhong Gao of Advanced Analysis & Testing Center, Nanjing Forestry University for providing valuable guidance on the use of SEM and AFM, respectively, and Jiahui Xu of Nanjing Forestry University for schematic illustration design.

References

Agarwal, U.P., Ralph, S.A., Baez, C., Reiner, R.S., Verrill, S.P., 2017. Effect of sample moisture content on XRD-estimated cellulose crystallinity index and crystallite size. Cellulose 24, 1971–1984. https://doi.org/10.1007/s10570-017-1259-0.

Alemdar, A., Sain, M., 2008. Isolation and characterization of nanofibers from agricultural residues: wheat straw and soy hulls. Bioresour. Technol. 99, 1664–1671. https://doi.org/10.1016/j.biortech.2007.04.029.

Ardanuy, M., Antunes, M., Velasco, J.I., 2012. Vegetable fibres from agricultural residues as thermo-mechanical reinforcement in recycled polypropylene-based green foams. Waste Manage. 32, 256–263. https://doi.org/10.1016/j.wasman.2011.09.022.

Barbash, V.A., Yaschenko, O.V., Shniruk, O.M., 2017. Preparation and properties of nanocellulose from organosolv straw pulp. Nanoscale Res. Lett. 12, 241. https://doi.org/10.1186/s11671-017-2001-4.

Bian, H., Chen, L., Gleisner, R., Dai, H., Zhu, J.Y., 2017. Producing wood-based nanomaterials by rapid fractionation of wood at 80 °C using a recyclable acid hydrotrope. Green Chem. 19, 3370–3379. https://doi.org/10.1039/C7GC00669A.

Bian, H., Gao, Y., Wang, R., Liu, Z., Wu, W., Dai, H., 2018a. Contribution of lignin to the surface structure and physical performance of cellulose nanofibrils film. Cellulose 25 (2), 1309–1318. https://doi.org/10.1007/s10570-018-1658-x.

Bian, H., Gao, Y., Yang, Y., Fang, G., Dai, H., 2018b. Improving cellulose nanofibrillation of waste wheat straw using the combined methods of prewashing, p-toluenesulfonic acid hydrolysis, disk grinding, and endoglucanase post-treatment. Bioresour. Technol. 256, 321–327. https://doi.org/10.1016/j.biortech.2018.02.038.

Bian, H., Wu, X., Luo, J., Qiao, Y., Fang, G., Dai, H., 2019. Valorization of alkaline peroxide mechanical pulp by metal chloride-assisted hydrotropic pretreatment for enzymatic saccharification and cellulose nanofibrillation. Polymers 11, 331. https://doi.org/10.3390/polym11020331.

Chandra, J., George, N., Narayanankutty, S.K., 2016. Isolation and characterization of cellulose nanofibrils from arecanut husk fibre. Carbohydr. Polym. 142, 158–166. https://doi.org/10.1016/j.carbpol.2016.01.015.

Chen, L., Dou, J., Ma, Q., Li, N., Wu, R., Bian, H., Yelle, D.J., Vuorinen, T., Fu, S., Pan, X., Zhu, J.Y., 2017. Rapid and near-complete dissolution of wood lignin at ≤80 °C by a recyclable acid hydrotrope. Sci. Adv. 3,. https://doi.org/10.1126/sciadv.1701735 e1701735.

Chen, L., Zhou, X., Shi, Y., Gao, B., Wu, J., Kirk, T.B., Xu, J., Xue, W., 2018. Green synthesis of lignin nanoparticle in aqueous hydrotropic solution toward broadening the window for its processing and application. Chem. Eng. J. 346, 217–225. https://doi.org/10.1016/j.cej.2018.04.020.

Chen, M., Zhang, X., Liu, C., Sun, R., Lu, F., 2014. Approach to renewable lignocellulosic biomass film directly from bagasse. ACS Sustain. Chem. Eng. 2, 1164–1168. https://doi.org/10.1021/sc400555v.

Cypriano, D.Z., da Silva, L.L., Tasic, L., 2018. High value-added products from the orange juice industry waste. Waste Manage. 79, 71–78. https://doi.org/10.1016/j.wasman.2018.07.028.

de Hoyos-Martinez, P.L., Erdocia, X., Charrier-El Bouhtoury, F., Prado, R., Labidi, J., 2018. Multistage treatment of almonds waste biomass: characterization and assessment of the potential applications of raw material and products. Waste Manage. 80, 40–50. https://doi.org/10.1016/j.wasman.2018.08.051.

Farooq, M., Zou, T., Riviere, G., Sipponen, M.H., Österberg, M., 2019. Strong, ductile, and waterproof cellulose nanofibril composite films with colloidal lignin particles. Biomacromolecules 20, 693–704. https://doi.org/10.1021/acs.biomac.8b01364.

Herrera, M., Thitiwutthisakul, K., Yang, X., Rujitanaroj, P.O., Rojas, R., Berglund, L., 2018. Preparation and evaluation of high-lignin content cellulose nanofibrils from eucalyptus pulp. Cellulose 25 (5), 3121–3133. https://doi.org/10.1007/s10570-018-1764-9.

Hietala, M., Varrio, K., Berglund, L., Soini, J., Oksman, K., 2018. Potential of municipal solid waste paper as raw material for production of cellulose nanofibres. Waste Manage. 80, 319–326. https://doi.org/10.1016/j.wasman.2018.09.033.

Huang, C., Wu, X., Huang, Y., Lai, C., Li, X., Yong, Q., 2016. Prewashing enhances the liquid hot water pretreatment efficiency of waste wheat straw with high free ash content. Bioresour. Technol. 219, 583–588. https://doi.org/10.1016/j.biortech.2016.08.018.

Inglesby, M.K., Zeronian, S.H., 2002. Direct dyes as molecular sensors to characterize cellulose substrates. Cellulose 9 (1), 19–29. https://doi.org/10.1023/A:1015840111614.

Jebali, Z., Nabili, A., Majdoub, H., Boufi, S., 2018. Cellulose nanofibrils (CNFs) from Ammophila arenaria, a natural and a fast growing grass plant. Int. J. Biol. Macromol. 107, 530–536. https://doi.org/10.1016/j.ijbiomac.2017.09.024.

Kaushik, A., Singh, M., 2011. Isolation and characterization of cellulose nanofibrils from wheat straw using steam explosion coupled with high shear homogenization. Carbohydr. Res. 346, 76–85. https://doi.org/10.1016/j.carres.2010.10.020.

Liu, Q., Lu, Y., Aguedo, M., Jacquet, N., Ouyang, C., He, W., Yan, C., Bai, W., Guo, R., Goffin, D., Song, J., Richel, A., 2017. Isolation of high-purity cellulose nanofibers from wheat straw through the combined environmentally friendly methods of steam explosion, microwave-assisted hydrolysis, and microfluidization. ACS

Sustain. Chem. Eng. 5, 6183–6191. https://doi.org/10.1021/acssuschemeng.7b01108.

Oliveira, F.B.D., Bras, J., Pimenta, M.T.B., Curvelo, A.A.D.S., Belgacem, M.N., 2016. Production of cellulose nanocrystals from sugarcane bagasse fibers and pith. Ind. Crops Prod. 93, 48–57. https://doi.org/10.1016/j.indcrop.2016.04.064.

Rajinipriya, M., Nagalakshmaiah, M., Robert, M., Elkoun, S., 2018. Importance of agricultural and industrial waste in the field of nanocellulose and recent industrial developments of wood based nanocellulose: a review. ACS Sustain. Chem. Eng. 6, 2807–2828. https://doi.org/10.1021/acssuschemeng.7b03437.

Rojo, E., Peresin, M.S., Sampson, W.W., Hoeger, I.C., Vartiainen, J., Laine, J., Rojas, O.J., 2015. Comprehensive elucidation of the effect of residual lignin on the physical, barrier, mechanical and surface properties of nanocellulose films. Green Chem. 17 (3), 1853–1866. https://doi.org/10.1039/C4GC02398F.

Segal, L., Creely, J.J., Martin, A.E., Conrad, C.M., 1959. An empirical method for estimating the degree of crystallinity of native cellulose using the X-Ray diffractometer. Text. Res. J. 29, 786–794. https://doi.org/10.1177/004051755902901003.

Shi, S., Zhang, M., Ling, C., Hou, W., Yan, Z., 2018. Extraction and characterization of microcrystalline cellulose from waste cotton fabrics via hydrothermal method. Waste Manage. 82, 139–146. https://doi.org/10.1016/j.wasman.2018.10.023.

Sluiter, A., Hames, B., Ruiz, R., Scarlata, C., Sluiter, J., Templeton, D., 2008a. Determination of Ash in Biomass. NREL Chemical Analysis and Testing Laboratory Analytical Procedures. Golden CO., NREL. NREL/TP-510-42622.

Sluiter, A., Hames, B., Ruiz, R., Scarlata, C., Sluiter, J., Templeton, D., 2008b. Determination of structural carbohydrates and lignin in biomass. NREL Chemical Analysis and Testing Laboratory Analytical Procedures. Golden CO, NREL. NREL/TP-510-42618.

Spence, K.L., Venditti, R.A., Habibi, Y., Rojas, O.J., Pawlak, J.J., 2010a. The effect of chemical composition on microfibrillar cellulose films from wood pulps: mechanical processing and physical properties. Bioresour. Technol. 101, 5961–5968. https://doi.org/10.1016/j.biortech.2010.02.104.

Spence, K.L., Venditti, R.A., Rojas, O.J., Habibi, Y., Pawlak, J.J., 2010b. The effect of chemical composition on microfibrillar cellulose films from wood pulps: water interactions and physical properties for packaging applications. Cellulose 17, 835–848. https://doi.org/10.1007/s10570-010-9424-8.

Su, Z., Bu, L., Zhao, D., Sun, R., Jiang, J., 2012. Processing of Lespedeza stalks by pretreatment with low severity steam and post-treatment with alkaline peroxide. Ind. Crops Prod. 36, 1–8. https://doi.org/10.1016/j.indcrop.2011.09.001.

Tarrés, Q., Espinosa, E., Domínguez-Robles, J., Rodríguez, A., Mutjé, P., Delgado-Aguilar, M., 2017. The suitability of banana leaf residue as raw material for the production of high lignin content micro/nano fibers: from residue to value-added products. Ind. Crops Prod. 99, 27–33. https://doi.org/10.1016/j.indcrop.2017.01.021.

Tripathi, A., Ferrer, A., Khan, S.A., Rojas, O.J., 2017. Morphological and thermochemical changes upon autohydrolysis and microemulsion treatments of coir and empty fruit bunch residual biomass to isolate lignin-rich micro- and nanofibrillar cellulose. ACS Sustain. Chem. Eng. 5, 2483–2492. https://doi.org/10.1021/acssuschemeng.6b02838.

Wang, R., Bian, H., Ji, H., Yang, R., 2018. Preparation of lignocellulose/graphene composite conductive paper. Cellulose 25 (10), 6139–6149. https://doi.org/10.1007/s10570-018-1998-6.

Zhu, H.L., Luo, W., Ciesielski, P.N., Fang, Z.J., Zhu, J.Y., Henriksson, G., Himmel, M.E., Hu, L.B., 2016. Wood-derived materials for green electronics, biological devices, and energy applications. Chem. Rev. 116, 9305–9374. https://doi.org/10.1021/acs.chemrev.6b00225.